

ARTICLE TYPE

Data-driven dynamic event-triggered load frequency control for multi-area interconnected power systems with random delays

Yuhao Chen¹ | Huarong Zhao¹ | Li Peng¹ | Hongnian Yu²

¹School of Internet of Things Engineering, Jiangnan University, Wuxi, Jiangsu, China

²School of Computing, Engineering and the Built Environment, Edinburgh Napier University, Edinburgh EH10 5DT, UK

Correspondence

Corresponding author Huarong Zhao, Jiangnan University, Wuxi, Jiangsu, China.
Email: hrzhao@jiangnan.edu.cn

Abstract

This paper investigates a load frequency control issue for multi-area interconnected unknown power systems with random communication delays. First, a model-free adaptive control scheme is established by building an equivalent data relationship model between area control error and corresponding control input. Then, a dynamic event-triggered scheme is designed to improve resource utilization and reduce computational burden. Furthermore, random communication delays in the feedback and forward channels are considered. The results show that the proposed method is independent of any model information about the power system, only using the controlled system's control input and output data. Several simulation results validate the effectiveness of the proposed control scheme.

KEYWORDS

Load frequency control, Model-free adaptive control, Dynamic event-triggered strategy, Random communication delays

1 | INTRODUCTION

Load frequency control is a well-known method to balance the load demand and frequency of multi-area interconnected power systems. Numerous studies have demonstrated that load frequency control can enhance the overall performance of power systems¹. However, improper load frequency control can have significant consequences, including damage to power supply equipment or even explosions. In order to enhance the control performance, pioneering researchers employed model-based approaches^{2,3,4}, which have yielded promising results. A significant limitation of these approaches is their dependence on precise information of the system model. To address this, subsequent researchers proposed model estimation techniques that mitigate the reliance on exact model information^{5,6,7}. However, these methods also encounter new challenges. Applying model estimation techniques introduces additional estimation errors, which may result in unsatisfactory control performance when the estimation error is substantial. Furthermore, when the models are extensive and sophisticated, the computation and time required for model prediction will be significantly augmented.

In order to circumvent the necessity for a system model, the model-free adaptive control (MFAC) method has been proposed and implemented in a multitude of fields, such as multi-agent systems^{8,9}, trajectory tracking system¹⁰, magnetic levitation system¹¹, excitation velocity tracking for robotic surface vehicles¹², and unmanned aerial vehicle¹³. The fundamental MFAC model collects system's input and output data to construct a data-relationship model by applying dynamic linearization and pseudo-partialization techniques. Concurrently, scholars are engaged in the development of novel MFAC algorithms^{14,15,16,17,18}. Zheng et al.¹⁴ developed a model-adaptive distributed optimization algorithm for generic nonlinear model-free multi-agent systems. Segheri et al.¹⁵ proposed a model-free adaptive backstepping control for a class of uncertain nonlinear systems. Weng et al.¹⁶ addressed the fast trajectory tracking problem for discrete-time nonlinear systems. The properties above of MFAC render it an optimal choice for use in load frequency control, mainly when the system model is intricate and challenging to obtain.

Nevertheless, the application of MFAC control in power systems has not yet received significant attention, which is one of the motivations for this study.

Despite the advantages of MFAC, the computation of feasible solutions for the control gain will impose a high real-time computational burden. Event-triggered algorithms have been implemented to address this challenge, where the control signal is updated and transmitted only when a specific condition is met. Many researchers proposed static event-triggered algorithms with fixed trigger conditions^{19,20,21,22}, which have been demonstrated to achieve great results. Some scholars proposed the use of a switching event triggering algorithm, which involves switching between different triggering conditions according to the system state^{24,25}. Moreover, dynamic event trigger algorithms have been proposed, in which the trigger conditions are adjusted according to the system state^{26,27,28}. However, most existing event-triggered methods are static event-triggered methods, especially for load frequency control with MFAC. Hence, further investigating a dynamic event-triggered MFAC method for a power system is challenging.

In addition, due to the increasing scale and complexity of the power system, the deployment cost and reliability of the distributed network control system face significant challenges¹. Cloud-based network control systems become more promising with the advancement of communication technology. This paper deploys the control systems to the cloud, which increases computing power and saves the cost of distributed deployment. However, it is accompanied by the problem of random communication delays when the communication environment is imperfect. Regarding random delays, researchers have done related studies in numerous fields, such as magnetic levitation trains²⁹, electric power systems³⁰, and uncertain nonlinear networked systems³¹. Lu et al.³² studied the exponential stability of impulsive control systems with random delays. Shang et al.³⁰ presented a networked predictive control method to predict the control signals. Zhang et al.³³ quantitatively represented the random time delays in a discrete way.

Motivated by the aforementioned problems, this paper studies the dynamic event-triggered model-free adaptive control (DETMFAC) for the load frequency control problem in multi-area interconnected power systems under random round-trip time delays. The main contributions of this paper are summarized below.

1. Develop a MFAC based load frequency control scheme for multi-area interconnected power systems that eliminates the need to use the power system model information. Unlike Wang et al.⁶ and Qi et al.⁷, this paper avoids introducing model estimation errors by using only the input and output data data.
2. Present a data-driven dynamic event-triggered strategy for load frequency control. Compared with the existing event-trigger strategies in the works^{19,20,21}, proposed strategy can further reduce the number of trigger times and ensure the stability of the system.
3. Propose an input design-based compensation control method that considers both the feedback and forward channels. In contrast to the compensation control schemes in the works^{30,34,35}, the random communication delays in both the feedback and forward channels are considered and compensated.

The rest of this article is organized as follows: Section 2 modifies the multi-area power system and introduces the DETMFAC and input design-based compensation control schemes. Section 3 illustrates the stability analysis. Section 4 gives the simulation results. Finally, Section 5 concludes this paper.

2 | DESIGN OF DETMFAC AND COMPENSATION CONTROL SCHEME

2.1 | Modeling of Multi-area Power System

Refer to Bu et al.²³, the dynamic model of i th power system is described as

$$\begin{cases} \Delta \dot{f}_i(t) = -\frac{D_i}{M_i} \Delta f_i(t) - \frac{1}{M_i} \Delta P_{\text{tie}-i}(t) \\ \quad + \frac{1}{M_i} (\Delta P_{mi}(t) - \Delta P_{di}(t)) \\ \Delta \dot{P}_{\text{tie}-i}(t) = 2\pi \sum_{j=1, j \neq i}^N T_{ij} \Delta f_i(t) - 2\pi \sum_{j=1, j \neq i}^N T_{ij} \Delta f_j(t). \\ \Delta \dot{P}_{mi}(t) = -\frac{1}{T_{ti}} P_{mi}(t) + \frac{1}{T_{ti}} P_{gi}(t) \\ \Delta \dot{P}_{gi}(t) = -\frac{1}{R_i T_{gi}} \Delta f_i(t) - \frac{1}{T_{gi}} P_{gi}(t) + \frac{1}{T_{gi}} \Delta P_{ci}(t) \end{cases}$$

Based on the Euler approximation law, The discrete-time model of i th power system is described as

$$\begin{cases} x_i(k+1) = G_i x_i(k) + H_i u_i(k) + W_i \vartheta_i(k) \\ \text{ACE}_i(k) = C_i x_i(k) \end{cases} \quad (1)$$

where $x_i(k) = [\Delta f_i(k) \Delta P_{\text{tie}-i}(k) \Delta P_{mi}(k) \Delta P_{gi}(k)]^T$ is the state vector, k denotes the discrete instant, $u_i(k) = \Delta P_{ci}(k)$ is defined as the system's input variable and the disturbance vector is $\vartheta_i^T(k) = [\Delta P_{di}(k) \sum_{j=1, j \neq i}^N T_{ij} \Delta f_j(k)]$. $W_i = \int_0^T e^{A_i t} F_i dt$, $H_i = \int_0^T e^{A_i t} B_i dt$, and $G_i = e^{A_i T}$. Furthermore,

$$A_i = \begin{bmatrix} -\frac{D_i}{M_i} & -\frac{1}{M_i} & \frac{1}{M_i} & 0 \\ 2\pi \sum_{j=1, j \neq i}^N T_{ij} & 0 & 0 & 0 \\ 0 & 0 & -\frac{1}{T_{ti}} & \frac{1}{T_{ti}} \\ -\frac{1}{R_i T_{gi}} & 0 & 0 & -\frac{1}{T_{gi}} \end{bmatrix}$$

$$B_i = \begin{bmatrix} 0 & 0 & 0 & \frac{1}{T_{gi}} \end{bmatrix}^T \quad C_i = [\beta_i \ 1 \ 0 \ 0]$$

and

$$F_i = \begin{bmatrix} -\frac{1}{M_i} & 0 & 0 & 0 \\ 0 & -2\pi & 0 & 0 \end{bmatrix}^T$$

In this article, the parameters are given in Table 1 and matrices G_i , H_i , and W_i are unknown. The area control error signal of i th area is given as

$$\text{ACE}_i(k) = \beta_i \Delta f_i(k) + P_{\text{tie}-i}(k) \quad (2)$$

where $\beta_i = 1/R_i + D_i$ denotes the frequency bias factor. From Eq. (1), one can obtain that

$$\text{ACE}_i(k+1) = C_i G_i x(k) + C_i H_i u_i(k) + C_i W_i \vartheta_i(k) \quad (3)$$

Furthermore, $\text{ACE}_i(k+1)$ can be rewritten as

$$\text{ACE}_i(k+1) = f_i(\text{ACE}_i(k), u_i(k)) + \omega_i(k) \quad (4)$$

where $\omega_i(k) = C_i W_i \vartheta_i(k)$ is bounded disturbance. $f_i(\cdot)$ is an unknown nonlinear function. The nonlinear system (4) satisfies the following two assumptions.

Assumption 1. The partial derivative of $f_i(\cdot)$ with respect to $u_i(k)$ is continuous.

Assumption 2. The nonlinear system (4) satisfies the generalized Lipschitz condition, that is, for any $k \geq 0$, and $\Delta u_i(k) \neq 0$, there is

$$|\Delta \text{ACE}_i(k+1)| \leq b |\Delta u_i(k)| \quad (5)$$

where $\Delta \text{ACE}_i(k+1) = \text{ACE}_i(k+1) - \text{ACE}_i(k)$, $\Delta u_i(k) = u_i(k) - u_i(k-1)$, and $b > 0$.

Theorem 1. Under Assumptions 1 and 2, when $|\Delta u_i(k)| \neq 0$, the system can be transformed into the following compact form dynamic linearization model:

$$\Delta \text{ACE}_i(k+1) = \phi_i(k) \Delta u_i(k) + \Delta \omega_i(k) \quad (6)$$

where $\phi_i(k)$ is a time-varying parameter called pseudopartial derivative (PPD), and $\Delta \omega_i(k) = \omega_i(k) - \omega_i(k-1)$. $\phi_i(k)$ is an unknown time-varying parameter, which reflects the dynamic evolution relationship between control input $u_i(k)$ and systems output $\text{ACE}_i(k)$. Furthermore, since system (4) satisfies the generalized Lipschitz condition, we have $|\phi_i(k)| \leq b$ for any instant k .

Proof. : From the definition of $\text{ACE}_i(k+1)$ in Eq. (4), one has

$$\begin{aligned} \Delta \text{ACE}_i(k+1) &= f_i(\text{ACE}_i(k), u_i(k)) + \omega_i(k) - f_i(\text{ACE}_i(k-1), u_i(k-1)) - \omega_i(k-1) \\ &= f_i(\text{ACE}_i(k), u_i(k)) + \Delta \omega_i(k) - f_i(\text{ACE}_i(k), u_i(k-1)) \\ &\quad + f_i(\text{ACE}_i(k), u_i(k-1)) - f_i(\text{ACE}_i(k-1), u_i(k-1)). \end{aligned} \quad (7)$$

By employing Assumption 1 and Cauchy mean-value Theorem, Eq. (7) can be rewritten into the following form:

$$\Delta \text{ACE}_i(k+1) = \frac{\partial f_i^*}{\partial u_i(k)} \Delta u_i(k) + \psi_i(k) + \Delta \omega_i(k) \quad (8)$$

where

$$\begin{aligned} \psi_i(k) &= f_i(\text{ACE}_i(k), u_i(k-1)) \\ &\quad - f_i(\text{ACE}_i(k-1), u_i(k-1)) \end{aligned} \quad (9)$$

For each discrete time instant k , consider the following data equation with the variable $\varsigma_i(k)$:

$$\psi_i(k) = \varsigma_i(k) \Delta u_i(k) \quad (10)$$

Since $|\Delta u_i(k)| \neq 0$, there exists a unique solution $\varsigma_i^*(k)$ to Eq. (10). Denote $\phi_i(k) = \partial f_i^* / \partial u_i(k) + \varsigma_i^*(k)$, then Eq. (7) can be expressed as $\Delta \text{ACE}_i(k+1) = \phi_i(k) \Delta u_i(k) + \Delta \omega_i(k)$. The proof is completed. \square \square

2.2 | Data-Driven Control Algorithm

To design the data-driven load frequency control algorithm, the linearization data model in Theorem 1 is rewritten as

$$\text{ACE}_i(k+1) = \text{ACE}_i(k) + \phi_i(k) \Delta u_i(k) + \Delta \omega_i(k) \quad (11)$$

Consider the following criterion function of control input $u_i(k)$:

$$J(u_i(k)) = |\text{ACE}_d(k+1) - \text{ACE}_i(k+1)|^2 + \lambda_i |u_i(k) - u_i(k-1)|^2 \quad (12)$$

where $\lambda_i > 0$ is a weighting factor used to limit the changes of $u_i(k)$, and $\text{ACE}_d(k)$ is the desired output trajectory.

In the context of the communication graph depicted in Fig. 1, The controller computes control commands only when it receives a feedback packet, of which the timestamp is supposed to be $k_s \leq k$.

Substitute Eq. (11) into the criterion function and set the derivative of the criterion function with respect to $u_i(k)$ be zero. Accordingly, the following control algorithm can be obtained as

$$\Delta u_i(k_s) = \frac{\rho_i \phi_i(k_s)}{\lambda_i + |\phi_i(k_s)|^2} (\text{ACE}_d(k_s+1) - \text{ACE}_i(k_s)) \quad (13)$$

where $\rho_i \in (0, 1]$ is a step-size factor added to make the algorithm more general.

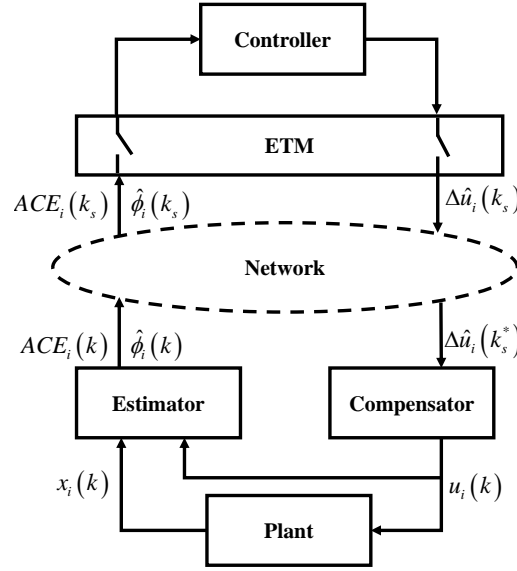


FIGURE 1 System block diagram with dynamic event-trigger and input design-based compensation control method.

In order to implement the control algorithm (13), the value of PPD needed to be known in advance. However, because the parameter matrices of the system are unknown, and PPD is a time-varying parameter, its exact value is difficult to obtain. As a result, an estimation algorithm of PPD is designed, and the criterion function is set as

$$J(\phi_i(k_s)) = |\text{ACE}_i(k_s) - \text{ACE}_i(k_s - 1) - \phi_i(k_s) \Delta u_i(k_s - 1)|^2 + \mu_i |\phi_i(k_s) - \hat{\phi}_i(k_s - 1)|^2 \quad (14)$$

where $\mu_i > 0$ is a weighing factor. $\hat{\phi}_i(k)$ is the estimation value of $\phi_i(k)$. The method similar to one above is adopted to minimize the criterion function (12). Then, an estimation algorithm of PPD can be obtained

$$\Delta \hat{\phi}_i(k_s) = \left(\Delta \text{ACE}_i(k_s) - \hat{\phi}_i(k_s - 1) \Delta u_i(k_s - 1) \right) \times \frac{\eta_i \Delta u_i(k_s - 1)}{\mu_i + \Delta u_i(k_s - 1)^2} \quad (15)$$

where η_i denotes a step-size factor. To ensure the invariability of frequency and interchange power, the desired value of area control error signal is set as $\text{ACE}_d(k) = \text{const} = 0$.

2.3 | Dynamic Event-Triggered Mechanism

The designed MFAC algorithm is predicated on the assumption that the network will engage in continuous communication. However, the network resources are finite, and continuous communication will waste them. A dynamic event-triggered mechanism has been introduced to mitigate this issue. Subsequently, a dynamic event-triggered function is designed as

$$\theta_i(k) = \frac{1}{v_i} |\varphi_i(k)| + m_i - |e_i^r(k_s)| \quad (16)$$

where $e_i^r(k_s) = e_i(k_{i,r}) - e_i(k_s)$ represents the triggering error. $k_{i,r}$ is the latest event-triggered instant. $e_i(k) = \text{ACE}_d - \text{ACE}_i(k)$ denotes the tracking error. It is clear that for the triggering instant, $e_i^r(k)$ is equal to zero. v_i and m_i are positive constants and can be set as desired. $\varphi_i(k)$ represents the dynamic variable satisfying

$$\varphi_i(k+1) = \gamma_i \varphi_i(k) + m_i - |e_i^r(k)|, \varphi_i(1) = \varphi_0 \quad (17)$$

where $\gamma_i > 0$ and φ_0 are the designed parameter and initial value, respectively.

The event-triggered condition is designed as

$$k_{i,r+1} = \inf \{k \in \mathbb{N} \mid k > k_{i,r}, \theta_i(k) < 0\} \quad (18)$$

Then, a DETMFAC scheme for the i th area is developed as follows:

$$\Delta \hat{\phi}_i(k) = \begin{cases} \frac{\eta_i \Delta u_i(k_s - 1)}{\mu_i + \Delta u_i(k_s - 1)^2} \\ \times \left(\frac{\Delta ACE_i(k_s)}{-\hat{\phi}_i(k_s - 1) \Delta u_i(k_s - 1)} \right), k_s = k_{i,r} \\ 0, k_s \in (k_{i,r-1}, k_{i,r}) \end{cases} \quad (19)$$

$$\hat{\phi}_i(k) = \hat{\phi}_i(1), \text{ if } |\hat{\phi}_i(k)| \leq \varepsilon, \text{ or } |\Delta u_i(k_s^* - 1)| \leq \varepsilon \quad (20)$$

$$\Delta \hat{u}_i(k_s) = \begin{cases} \frac{\rho_i \hat{\phi}_i(k_s)}{\lambda_i + |\hat{\phi}_i(k_s)|^2} (ACE_d - ACE_i(k_s)), k_s = k_{i,r} \\ 0, k_s \in (k_{i,r-1}, k_{i,r}) \end{cases} \quad (21)$$

where ε is a small positive constant, and $\hat{\phi}_i(1)$ is the initial value of $\hat{\phi}_i(k)$.

Remark 1. Eq. (13) indicates that, with $\phi_i(k_s) > 0$, $\phi_i(k_s + 1) > 0$, and $\lambda_i > 0$, we can obtain that $\text{sign}(\Delta u_i(k_s + 1)) = \text{sign}(\Delta u_i(k_s))$, and further $|\Delta u_i(k_s + 1)| < |\Delta u_i(k_s)|$ if $\phi_i(k_s + 1) \approx \phi_i(k_s)$, which will inspire us in the following to design a compensator in the actuator.

2.4 | Input Design-based Compensation Control

In the actuator, a compensator is designed (see Fig. 1) to buffer the received packets and only store the latest packet through the comparison of timestamps and to compensate for random network-induced delays based on the latest packet. For our purpose, the effect of the network-induced delays in both channels is described by redefining the round trip time delays τ_k as

$$\tau_k = k - k_s^* \quad (22)$$

where k_s^* is the timestamp of the latest packet with $k_s^* \leq k_s \leq k$. Thus, the latest control increment available in the actuator can be expressed as $\Delta \hat{u}(k_s^*)$.

It is assumed that the round trip time delay τ_k is bounded by $\bar{\tau}$, i.e., $\tau_k \leq \bar{\tau}$ for all k , which means that at least one packet can arrive at the actuator during $\bar{\tau}$ sampling periods. According to the fact mentioned in Remark 1, a network delays compensation strategy based on the control input design is presented as follows:

$$\Delta u_i(k) = \Gamma_i^{\tau_k} \Delta \hat{u}_i(k_s^*) \quad (23)$$

where $\Gamma_i > 0$ is the compensation factor. Then we have

$$u_i(k) = u_i(k_s^* - 1) + \sum_{t=0}^{\tau_k} \Gamma_i^t \Delta \hat{u}_i(k_s^*). \quad (24)$$

3 | STABILITY ANALYSIS

This section studies the stabilization of multi-area interconnected power systems under the DETMFAC and input design-based compensation control schemes. Before presenting the primary results, it is necessary to give an assumption presented here.

Assumption 3. For any instant k and $\Delta u_i(k) \neq 0$, the sign of PPD remains unchanged, that is $\phi_i(k) > \bar{b}_i > 0$, where \bar{b}_i denotes a small positive constant.

Theorem 2. Consider that event-triggered data-driven load frequency control algorithm Eq. (19)-(21) is used for the unknown systems model (4). For the given task $\text{ACE}_d = 0$, when conditions $0 < \gamma_i + 1/v_i < 1$ and $2 - \sqrt{2} < \rho_i/\sqrt{\lambda_i} < 2$ hold, the tracking error $e_i(k)$ is convergent and the ultimate upper bound of the tracking errors is related to the bound of $|\Delta\omega_i(k)|$.

Proof. : Defining the estimation error $\delta_i(k) = \hat{\phi}_i(k) - \phi_i(k)$ and subtracting $\delta_i(k)$ from both sides of Eq. (15), one has

$$\begin{aligned}\delta_i(k) &= \phi_i(k-1) - \phi_i(k) + \delta_i(k-1) + \frac{\eta_i \Delta u_i(k-1)}{\mu_i + \Delta u_i(k-1)^2} \times \left(\Delta \text{ACE}_i(k) - \hat{\phi}_i(k-1) \Delta u_i(k-1) \right) \\ &= \phi_i(k-1) - \phi_i(k) + \delta_i(k-1) + \frac{\eta_i \Delta u_i(k-1)^2}{\mu_i + \Delta u_i(k-1)^2} \times \left(\phi_i(k-1) - \hat{\phi}_i(k-1) + \frac{\Delta \omega_i(k-1)}{\Delta u_i(k-1)} \right) \\ &= \phi_i(k-1) - \phi_i(k) + \delta_i(k-1) + \frac{\eta_i \Delta u_i(k-1)^2}{\mu_i + \Delta u_i(k-1)^2} \delta_i(k-1) + D_i\end{aligned}\quad (25)$$

where $D_i = \frac{\eta_i \Delta u_i(k-1)}{\mu_i + \Delta u_i(k-1)^2} \Delta \omega_i(k-1)$. Taking the absolute value of Eq. (25), one can obtain

$$|\delta_i(k)| \leq \left| 1 - \frac{\eta_i \Delta u_i(k-1)^2}{\mu_i + \Delta u_i(k-1)^2} \right| \times |\delta_i(k-1)| + |\phi_i(k-1) - \phi_i(k)| + |D_i|$$

Due to the reset policy, the minimum of $\frac{\eta_i \Delta u_i(k-1)^2}{\mu_i + \Delta u_i(k-1)^2}$ is $\frac{\eta_i \varepsilon^2}{\mu_i + \varepsilon^2}$. One has $\left| 1 - \frac{\eta_i \Delta u_i(k-1)^2}{\mu_i + \Delta u_i(k-1)^2} \right| \leq 1 - \frac{\eta_i \varepsilon^2}{\mu_i + \varepsilon^2} \triangleq d_i < 1$. From Theorem 1, we have $|\phi_i(k)| \leq b$. Thus, $|\phi_i(k-1) - \phi_i(k)| \leq 2b$. Then, according to Eq. (25), we have

$$\begin{aligned}|\delta_i(k)| &\leq d_i |\delta_i(k-1)| + 2b + D_i \\ &\leq d_i^2 |\delta_i(k-2)| + 2d_i b + 2b + d_i D_i + D_i \\ &\leq \dots \\ &\leq d_i^k |\delta_i(0)| + \frac{1 - d_i^k}{1 - d_i} (2b + D_i)\end{aligned}\quad (26)$$

which means that $\delta_i(k)$ is uniformly bounded. Considering the boundedness of $\phi_i(k)$ in Theorem 1, $\delta_i(k)$ is bounded.

Now we proof the boundedness of $\varphi_i(k)$.

$$\begin{aligned}|\varphi_i(k+1)| &\leq \gamma_i |\varphi_i(k)| + m_i + |e_i^r(k)| \\ &\leq \gamma_i |\varphi_i(k)| + m_i + \frac{1}{v_i} |\varphi_i(k)| + m_i \\ &\leq \left(\gamma_i + \frac{1}{v_i} \right) |\varphi_i(k)| + 2m_i \\ &\leq \left(\gamma_i + \frac{1}{v_i} \right)^2 |\varphi_i(k-1)| + 2 \left(\gamma_i + \frac{1}{v_i} \right) m_i + 2m_i \\ &\vdots \\ &\leq \left(\gamma_i + \frac{1}{v_i} \right)^k |\varphi_i(1)| + \frac{2m_i \left[1 - \left(\gamma_i + \frac{1}{v_i} \right)^k \right]}{1 - \left(\gamma_i + \frac{1}{v_i} \right)}\end{aligned}\quad (27)$$

When conditions hold, $\varphi_i(k)$ converges to the following set:

$$\left\{ \varphi_i(k) \mid |\varphi_i(k)| \leq \frac{2m_i}{1 - (\gamma_i + 1/v_i)} \right\}\quad (28)$$

Now we proof the boundedness of tracking error $e_i(k)$. The $e_i(k+1)$ can be rewritten as

$$\begin{aligned}e_i(k+1) &= e_i(k) - \phi_i(k) \Delta u_i(k) - \Delta \omega_i(k) \\ &= (1 - \Phi_i(k)) e_i(k) - \Delta \omega_i(k)\end{aligned}\quad (29)$$

where $\Phi_i(k) = \frac{\rho_i \hat{\phi}_i(k)}{\lambda_i + |\hat{\phi}_i(k)|^2}$, the Lyapunov function is defined as $V_i(k+1) = e_i^2(k+1)$, and one has

$$\begin{aligned}\Delta V_i(k+1) &= V_i(k+1) - V_i(k) \\ &= e_i^2(k+1) - e_i^2(k)\end{aligned}\quad (30)$$

Substituting $e_i(k+1)$ into Eq. (30), one has

$$\begin{aligned}\Delta V_i(k+1) &= ((1 - \Phi_i(k)) e_i(k) - \Delta \omega_i(k))^2 - e_i^2(k) \\ &= (2(1 - \Phi_i(k))^2 - 1) V_i(k) + 8b_{\omega_i}^2\end{aligned}\quad (31)$$

If conditions hold, there exists a const $\Xi \in (0, 1)$ makes

$$0 < \left| \frac{\rho_i}{\lambda_i + |\hat{\phi}_i(k)|^2} \right| \leq \left| \frac{\rho_i \hat{\phi}_i(k)}{2\hat{\phi}_i(k) \sqrt{\lambda_i}} \right| = \left| \frac{\rho_i}{2\sqrt{\lambda_i}} \right| < \Xi \leq 1 \quad (32)$$

The Lyapunov function can be rewritten as

$$\begin{aligned}V_i(k+1) &= e_i^2(k+1) \\ &\leq \Xi V_i(k) + 8b_{\omega_i}^2 \\ &\leq \Xi^2 V_i(k-1) + 8\Xi b_{\omega_i}^2 + 8b_{\omega_i}^2 \\ &\vdots \\ &\leq \Xi^k V_i(1) + \frac{8b_{\omega_i}^2 (1 - \Xi^k)}{1 - \Xi}\end{aligned}\quad (33)$$

Due to $\Xi \in (0, 1)$ and $\lim_{k \rightarrow \infty} \Xi^k = 0$, $e_i(k)$ is bounded.

This ends the proof. \square

Next, the stability of the input design-based compensation control scheme is proved. The following introduces the necessary lemma:

Lemma 1. ³⁶ Consider the following discrete-time scalar system:

$$\begin{aligned}x(k+1) &= x(k) - \alpha(k)x(k - \tau_k), \\ x(k) &= \psi(k), k = -\bar{\tau}, -\bar{\tau} + 1, \dots, 0,\end{aligned}$$

where $x(k)$ is the scalar state, $\alpha(k)$ is the time-varying parameter, and $\psi(k)$ is the initial condition. The above system is stable if $0 < \alpha(k) < 2/(2\bar{\tau} + 1)$.

Theorem 3. If the following inequality holds

$$\Gamma_i < \sqrt{\tau_k \frac{(2 - (2\bar{\tau} + 1)\bar{\chi}_i) \left(\lambda_i + |\hat{\phi}_i(k - \tau_k)|^2 \right)}{(2\bar{\tau} + 1)\bar{\phi}_i \hat{\phi}_i(k - \tau_k)}} \quad (34)$$

the tracking error $e_i(k)$ is convergent and the power systems (4) are stable.

Proof. : The tracking error $e_i(k+1)$ can be rewritten as

$$\begin{aligned}e_i(k+1) &= e_i(k) - \Delta A C E_i(k+1) \\ &= e_i(k) - \phi_i(k) \Delta u_i(k) - \Delta \omega_i(k) \\ &= e_i(k) - \alpha_i(k) e_i(k - \tau_k) - \Delta \omega_i(k),\end{aligned}$$

with

$$\alpha_i(k) = \phi_i(k) \Gamma_i^{\tau_k} \frac{\rho_i \hat{\phi}_i(k - \tau_k)}{\lambda_i + \left| \hat{\phi}_i(k - \tau_k) \right|^2} + \chi_i \quad (35)$$

where $\chi_i = \Delta\omega_i(k)/e_i(k - \tau_k)$. Define $\bar{\phi}_i$ and $\bar{\chi}_i$ as the upper bound of ϕ_i and χ_i respectively. If Eq. (34) holds, we have

$$0 < \alpha_i(k) \leq \bar{\phi}_i \Gamma_i^{\tau_k} \frac{\rho_i \hat{\phi}_i(k - \tau_k)}{\lambda_i + \left| \hat{\phi}_i(k - \tau_k) \right|^2} + \bar{\chi}_i < \frac{2}{2\bar{\tau} + 1} \quad (36)$$

According to Lemma 1, $e_i(k)$ is bounded.

This end the proof. \square

4 | SIMULATION RESULTS

In order to verify the effectiveness of the proposed strategy, a simulation study is carried out to address the frequency fluctuation caused by initial load disturbance. Fig. 2 illustrates three identical interconnected control regions with a sampling period of 0.005s. Table 2 presents the selected parameter values. Moreover, $T_{12} = T_{21} = 0.20$ p.u./Hz, $T_{13} = T_{31} = 0.25$ p.u./Hz, and $T_{23} = T_{32} = 0.12$ p.u./Hz.

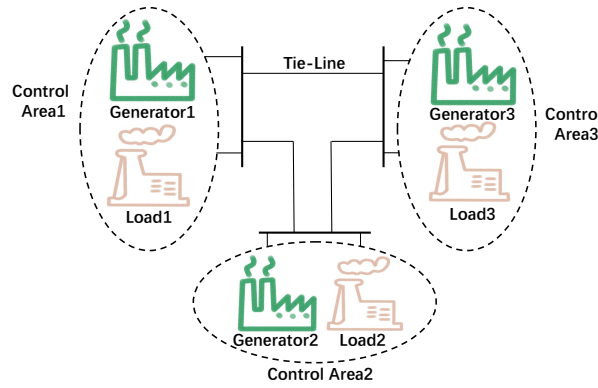


FIGURE 2 Three-area power system.

It should be emphasized that the established parameter values given in the simulation are only used to generate the necessary input and output data data for the controller.

4.1 | Example I

In this section, we demonstrate the control effectiveness of DETMFAC method and its ability to save communication resources under static load disturbances. The controller parameters are shown in Table 3. The power system's initial state is set to zero, and 0.02p.u. load step disturbances are added 5s later.

In Fig. 3, the output curves of power systems are plotted. As illustrated in Fig. 4, the horizontal coordinate represents the triggering moment, while the vertical coordinate represents the interval between two triggering moments. The proposed DETMFAC triggers 1,320 times, 9,79 times, and 1,270 times, saving 89.00%, 91.84%, and 89.41% communication resources in three areas, respectively. It is worth noting that the trigger times for area 1 in the work²³ is 6116 times, which represents that the method used in this paper can further reduce resource utilization.

As indicated in Fig. 5, the network round-trip time delays are observed to range between 0 and 4 seconds. Fig. 6 shows the dynamic event-triggered parameters θ_i of three areas.

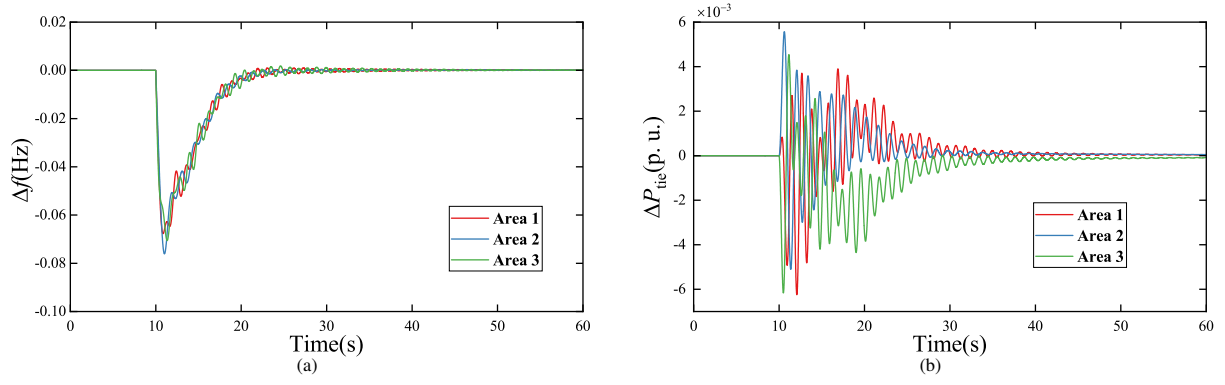


FIGURE 3 Response of Δf_i (a) and ΔP_{tie} (b) (example I).

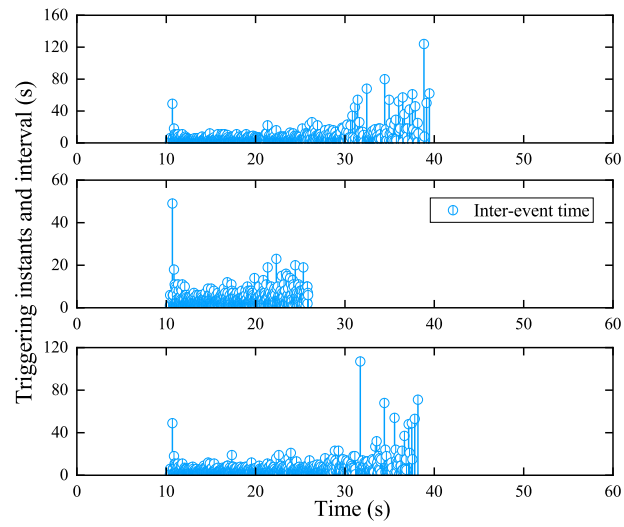


FIGURE 4 Triggering instants and intervals in three areas (example I).

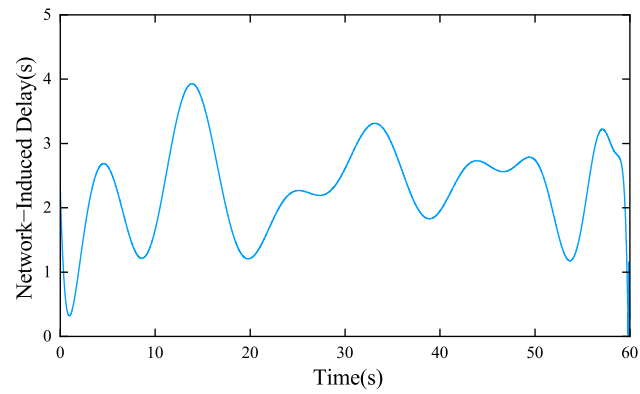


FIGURE 5 round trip time delays.

Fig. 7 and Fig. 8 show the Δf curves with different dynamic event-triggered and input compensation parameters. It should be noted that the system stability can not be ensured when $m_{1,2,3} = 0$ and $\Gamma_{1,2,3} = 0.75$. The former is due to few trigger times, while

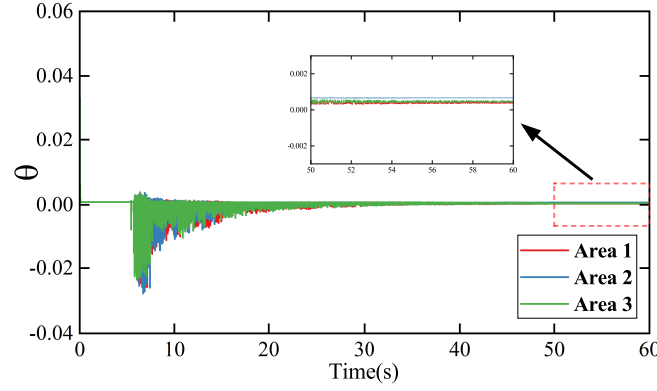


FIGURE 6 Trajectory of θ (example I).

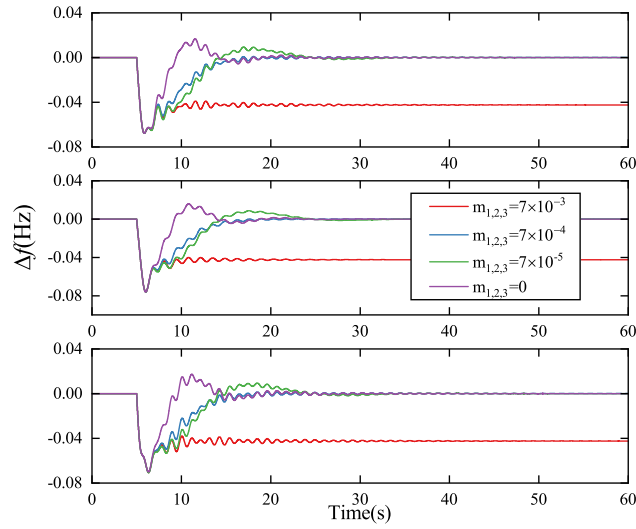


FIGURE 7 Response curves of Δf with different dynamic event-trigger parameters (example I).

the latter is attributed to the excessive compensation parameter, which leads to oscillations. The experimental data are listed in TABLE 2

4.2 | Example II

In this section, we demonstrate the effectiveness of proposed DETMFAC methods under dynamic load disturbances. The dynamic load disturbance $\Delta P_{di}(k) = 0.02 + 0.005\sin(k\pi/n)$ are added 5s after the system has commenced its simulation, n is the total sampling number.

In Fig. 9, the output curves of power systems are plotted. As illustrated in Fig. 10, the horizontal coordinate represents the triggering moment under dynamic load disturbances. The proposed DETMFAC triggers 4,214 times, 3,036 times, and 4,413 times, saving 64.88%, 74.70%, and 63.23% communication resources in three areas, respectively. Therefore, this method is effective under dynamic load disturbances.

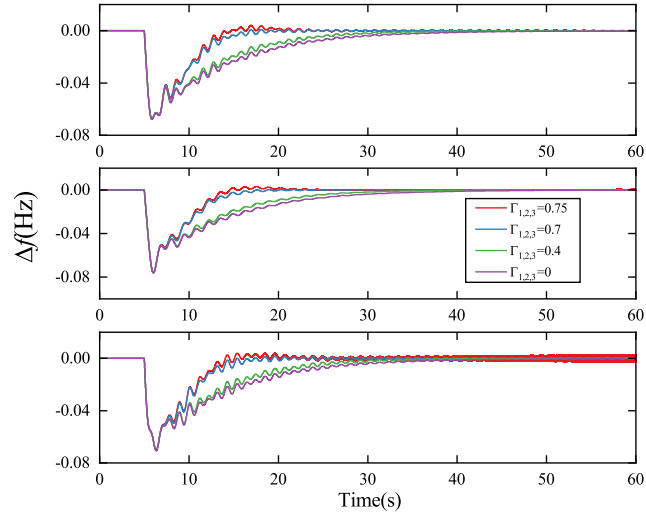


FIGURE 8 Response curves of Δf with different input compensation parameters (example I).

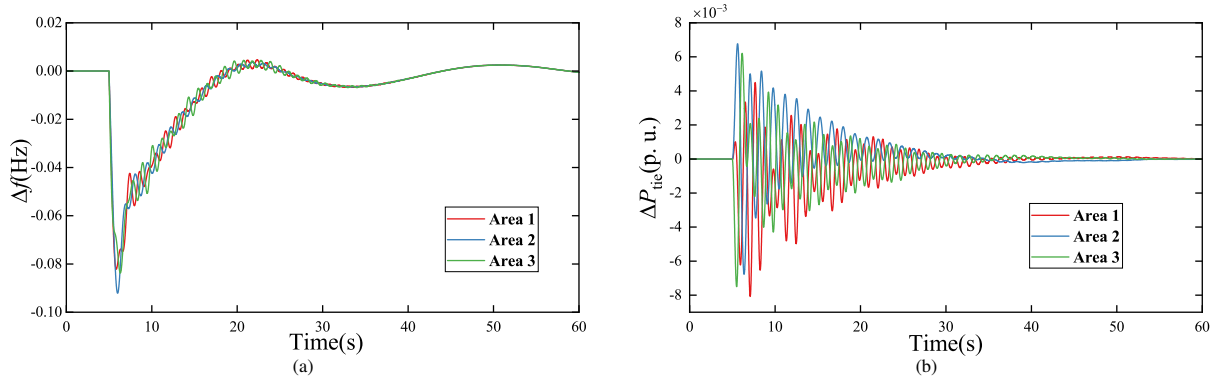


FIGURE 9 Response of Δf_i (a) and ΔP_{tie} (b) (example II).

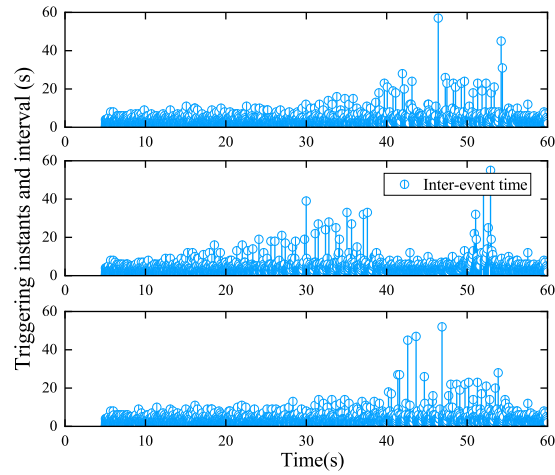


FIGURE 10 Triggering instants and intervals in three areas (example II).

5 | CONCLUSION

This paper designed a data-driven load frequency control approach for multi-area interconnected power systems. A dynamic event-triggered method and input design-based compensation control scheme have been designed for load frequency control. Compared with the existing methods, the proposed method can further reduce the communication burden and effects of dual-channel communication delays. The efficacy of the presented algorithm has been validated through a practical demonstration, and the control effects under varying parameters are contrasted. In the future, studying fixed-time load frequency control for multi-area interconnected power systems with input saturation will be challenging.

REFERENCES

1. Wadi M, Shobole A, Elmasry W, Kucuk I. Load frequency control in smart grids: a review of recent developments. *Renewable & Sustainable Energy Reviews*. 2024. doi: 10.1016/j.rser.2023.114013
2. Chen P, Liu S, Zhang D, Yu L. A deep asynchronous actor-critic learning-based event-triggered decentralized load frequency control of power systems with communication delays. *International Journal of Robust and Nonlinear Control*. 2022;32(5):3039-3061.
3. Li Y, Li X, Cheng J, Shi K, Qiu K. Reliable quantized sampled-data LFC for semi-Markov jump interconnected multi-area power systems: Dealing with incomplete TRs. *International Journal of Robust and Nonlinear Control*. 2024;34(5):3241-3258.
4. Yang F, He J, Wang D. New stability criteria of delayed load frequency control systems via infinite-series-based inequality. *IEEE Transactions on Industrial Informatics*. 2018;14(1):231-240.
5. Gulzar MM, Sibtain D, Khalid M. Cascaded fractional model predictive controller for load frequency control in multiarea hybrid renewable energy system with uncertainties. *International Journal of Energy Research*. 2023. doi: 10.1155/2023/5999997
6. Wang Y, Liu C, Liu Z, et al. A hierarchical cooperative frequency regulation control strategy of wind-storage-load in a microgrid based on model prediction. *Energies*. 2023;16(4):156-165.
7. Qi X, Zheng J, Mei F. Model predictive control-based load-frequency regulation of grid-forming inverter-based power systems. *Frontiers in Energy Research*. 2022. doi: 10.3389/fenrg.2022.932788
8. Zhao H, Shan J, Peng L, Yu H. Learning-based robust bipartite consensus control for a class of multiagent systems. *IEEE Transactions on Industrial Electronics*. 2023;70(4):4068-4076.
9. Bu X, Cui L, Yang P, Hou Z, Qian W. Formation control for a class of nonlinear multiagent systems using model-free adaptive iterative learning. *International Journal of Robust and Nonlinear Control*. 2018;28(4):1402-1412.
10. He D, Wang H, Tian Y. An α -variable model-free prescribed-time control for nonlinear system with uncertainties and disturbances. *International Journal of Robust and Nonlinear Control*. 2022;32(9):5673-5693.
11. Kang J, Huang X, Xia C, Huang D, Wang F. Ultralocal model-free adaptive supertwisting nonsingular terminal sliding mode control for magnetic levitation system. *IEEE Transactions on Industrial Electronics*. 2024;71(5):5187-5194.
12. Peng B, Gu N, Wang D, Peng Z. Model-free adaptive disturbance rejection control of an RSV with hardware-in-the-loop experiments. *IEEE Transactions on Industrial Electronics*. 2023;70(7):7507-7510.
13. Hao J, Zhang K, Zhang Z, Wang S, Shi C. An online model-free adaptive tracking controller for cable-driven medical continuum manipulators. *IEEE Transactions on Medical Robotics and Bionics*. 2023;5(3):623-635.
14. Zheng S, Liu S, Wang L. Event-triggered distributed optimization for model-free multi-agent systems. *Frontiers of Information Technology & Electronic Engineering*. 2024;25(2):214-224.
15. Segheri M, Boudjemaa F, Nemra A, Bibi Y. Model-free adaptive backstepping control for a class of uncertain nonlinear systems. *Transactions of the Institute of Measurement and Control*. 2024;46(7):1317-1330.
16. Weng Y, Zhang Q, Cao J, Yan H, Qi W, Cheng J. Finite-time model-free adaptive control for discrete-time nonlinear systems. *IEEE Transactions on Circuits and Systems II-Express Briefs*. 2023;70(11):4113-4117.
17. Zhao H, Yu H, Peng L. Event-triggered distributed data-driven iterative learning bipartite formation control for unknown nonlinear multiagent systems. *IEEE Transactions on Neural Networks and Learning Systems*. 2024;35:417-427.
18. Gao S, Zhao D, Yan X, Spurgeon SKK. Model-free adaptive state feedback control for a class of nonlinear systems. *IEEE Transactions on Automation Science and Engineering*. 2023. doi: 10.1109/tase.2023.3237811
19. Kazemy A, Lam J, Zhang XM. Event-triggered output feedback synchronization of master-slave neural networks under deception attacks. *IEEE Transactions on Neural Networks and Learning Systems*. 2022;33(3):952-961.
20. Zheng S, Shi P, Zhang H. Semiglobal periodic event-triggered output regulation for nonlinear multiagent systems. *IEEE Transactions on Automatic Control*. 2023;68(1):393-399.
21. Yao L, Huang X. Memory-based adaptive event-triggered secure control of markovian jumping neural networks suffering from deception attacks. *Science China-Technological Sciences*. 2023;66(2):468-480.
22. Tan Y, Yuan Y, Xie X, Tian E, Liu J. Observer-based event-triggered control for interval type-2 fuzzy networked system with network attacks. *IEEE Transactions on Fuzzy Systems*. 2023;31(8):2788-2798.
23. Bu X, Yu W, Cui L, Hou Z, Chen Z. Event-triggered data-driven load frequency control for multiarea power systems. *IEEE Transactions on Industrial Informatics*. 2022;18(9):5982-5991.
24. Cao L, Pan Y, Liang H, Huang T. Observer-based dynamic event-triggered control for multiagent systems with time-varying delay. *IEEE Transactions on Cybernetics*. 2023;53(5):3376-3387.
25. Zhou J, Xu D, Tai W, Ahn CK. Switched Event-triggered H_∞ security control for networked systems vulnerable to aperiodic dos attacks. *IEEE Transactions on Network Science and Engineering*. 2023;10(4):2109-2123.
26. Zhao H, Shan J, Peng L, Yu H. data-driven event-triggered formation of MIMO multiagent systems with constrained information. *IEEE Transactions on Systems Man Cybernetics-Systems*. 2024;54(1):39-49.
27. Wu J, Lu M, Deng F, Chen J. Event-triggered cooperative robust output regulation of minimum-phase linear uncertain multi-agent systems. *International Journal of Robust and Nonlinear Control*. 2024;34(11):7390-7405.

28. Zhao H, Shan J, Peng L, Yu H. Adaptive event-triggered bipartite formation for multiagent systems via reinforcement learning. *IEEE Transactions on Neural Networks and Learning Systems*. 2023. doi: 10.1109/tnnls.2023.3309326
29. Sun Y, Xu J, Chen C, Hu W. Reinforcement learning-based optimal tracking control for levitation system of maglev vehicle with input time delay. *IEEE Transactions on Instrumentation and Measurement*. 2022. doi: 10.1109/tim.2022.3142059
30. Shang XC, He Y, Zhang K, et al. Resilient load frequency control of power systems to compensate random time delays and time-delay attacks. *IEEE Transactions on Industrial Electronics*. 2023;70(5):5115-5128.
31. Karimi Z, Jalali A, Batmani Y. Event-triggered dynamic surface control of uncertain nonlinear networked systems subject to transmission delays. *International Journal of Robust and Nonlinear Control*. 2023;33(3):2479-2495.
32. Lu J, Jiang B, Zheng WX. Potential impacts of delay on stability of impulsive control systems. *IEEE Transactions on Automatic Control*. 2022;67(10):5179-5190.
33. Zhang X, Han Q, Ge X. A novel approach to H_∞ performance analysis of discrete-time networked systems subject to network-induced delays and malicious packet dropouts. *Automatica*. 2022. doi: 10.1016/j.automatica.2021.110010
34. Sun L, Xue W, Li D, Zhu H, Su Z. Quantitative tuning of active disturbance rejection controller for foptd model with application to power plant control. *IEEE Transactions on Industrial Electronics*. 2022;69(1):805-815.
35. Wang L, Xie L, Yang Y, Zhang Y, Wang K, Cheng S. Distributed online voltage control with fast pv power fluctuations and imperfect communication. *IEEE Transactions on Smart Grid*. 2023;14(5):3681-3695.
36. Pang Z, Liu G, Zhou D, Sun Dm Data-based predictive control for networked nonlinear systems with network-induced delay and packet dropout. *IEEE Transactions on Industrial Electronics*. 2016;63(2):1249-1257.

TABLE 1 SIGNALS OF THE i TH AREA SYSTEM

Symbol	Quantity
M_i	inertia of generator (p.u. s)
Δf_i	frequency deviation (Hz)
T_{ti}	turbine time constants (s)
ΔP_{tie-i}	tie line power deviation (p.u.)
T_{gi}	governor time constants (s)
T_{ij}	synchronizing torque coefficient of tie-line between two different areas (p.u./Hz)
ACE_i	area control error (ACE) (p.u.)
ΔP_{mi}	generator output power deviation (p.u.)
β_i	frequency bias factor (p.u./Hz)
D_i	generator unit damping coefficient (p.u./Hz)
ΔP_{gi}	governor valve position deviation (p.u.)
R_i	speed droop (Hz/p.u.)

TABLE 2 Relationship of Parameters and Transmission Quantity

$v_{1,2,3}$	$m_{1,2,3}$	Total triggering times	Transmission saving rate
15	7×10^{-3}	443	98.77%
15	7×10^{-4}	3,569	90.09%
15	7×10^{-5}	10,247	71.54%
15	0	15,405	58.21%

TABLE 3 PARAMETERS of POWER SYSTEMS

Parameters	Area 1	Area 2	Area 3
$D/(p.u./Hz)$	0.016	0.015	0.016
$M/(p.u. \cdot s)$	0.1677	0.2006	0.1236
$R/(Hz/p.u.)$	2.98	2.69	2.81
T_g/s	0.07	0.06	0.08
T_t/s	0.40	0.44	0.30
$\beta/(p.u./Hz)$	0.3479	0.3826	0.3689

TABLE 4 PARAMETERS of CONTROLLERS

Parameters	Area 1	Area 2	Area 3
ρ_i	0.84	0.86	0.83
μ_i	1.3	1.1	1.2
η_i	0.3	0.5	0.2
λ_i	1.1	1.2	1.3
ε_i	10^{-5}	10^{-5}	10^{-5}
v_i	15	15	15
m_i	7×10^{-3}	7×10^{-3}	7×10^{-3}
$\hat{\phi}_i(1)$	0.1	0.1	0.1
γ_i	0.7	0.7	0.7